



OPEN

# ZnO Nanorod Array Grown on Ag Layer: A Highly Efficient Fluorescence Enhancement Platform

SUBJECT AREAS:

BIOSENSORS

NANOSTRUCTURES

NANOWIRES

Yongqi Yin<sup>1</sup>, Ye Sun<sup>1</sup>, Miao Yu<sup>2</sup>, Xiao Liu<sup>1</sup>, Tingting Jiang<sup>2</sup>, Bin Yang<sup>1</sup>, Danqing Liu<sup>3</sup>, Shaoqin Liu<sup>3</sup> & Wenwu Cao<sup>1,4</sup>

Received

24 September 2014

Accepted

24 December 2014

Published

30 January 2015

Correspondence and requests for materials should be addressed to Y.S. (sunye@hit.edu.cn); M.Y. (miaoyu\_che@hit.edu.cn) or W.C. (dzk@psu.edu)

<sup>1</sup>Condensed Matter Science and Technology Institute, School of Science, Harbin Institute of Technology, Harbin 150080, China, <sup>2</sup>State Key Laboratory of Urban Water Resource and Environment, School of Chemical Engineering and Technology, Harbin Institute of Technology, Harbin 150001, China, <sup>3</sup>Key Laboratory of Microsystems and Microstructures Manufacturing, Harbin Institute of Technology, Harbin 150080, China, <sup>4</sup>Department of Mathematics and Materials Research Institute, The Pennsylvania State University, University Park, Pennsylvania 16802, USA.

**ZnO nanorods (NRs) are known for ultra-sensitive biomolecule detection through fluorescence enhancement. In this work, we demonstrate that ZnO NR arrays grown on Ag layers can significantly improve the enhancement up to 86 times compared to that grown on bare Si, and the enhancement can be modified in a controlled manner by varying Ag thickness. The much improved waveguide properties are attributed to the high reflectance of the Ag layers and their tuning effect on the diameters of ZnO NRs. Our results provide a deep insight into the mechanism of NRs-based fluorescence enhancement platform.**

Detection of fluorescence has become one of the most fascinating and preferred techniques in the field of biological sensing in recent years. To probe the fluorescence signal with an ultrahigh sensitivity, in addition to selecting brighter fluorophores and improving the spectrometers, major progress has been made on the signal enhancement by using functionalized substrates<sup>1–5</sup>. Very recently, ZnO nanorod (NR) array has been recognized as an appealing fluorescence enhancement (FE) platform for ultra-sensitive detection of biomolecules, due to its capability to detect DNA molecules, antiIgG or cancer biomarkers at a concentration down to a few femto-molar or pico-gmL<sup>-1</sup> level<sup>6–8</sup>. Factors primarily contributed to the enhancement have been proposed previously, including interfacial electron transfer<sup>9</sup>, large surface area of ZnO NRs<sup>10</sup> and their waveguide structures<sup>11</sup>, where the hexagonal structures of ZnO NRs can be regarded as Fabry-Perot resonators (FPRs) with the end faces as reflecting mirrors. The light-guiding properties have imparted ZnO NR arrays considerable application potentials in diverse photonic devices, such as optical sensors and nanowire lasers<sup>12,13</sup>.

The waveguide modes of inorganic NRs have been investigated both experimentally and theoretically<sup>3,14–16</sup>. It was shown that the fluorescence from the fluorophores near NRs can be captured and guided by waveguide structures<sup>12</sup>. Local field intensity in the vicinity of NRs enhanced by the resonance of the guided fundamental mode<sup>3,14</sup> and the evanescent field associated with the high-order modes<sup>15,16</sup> can significantly reinforce the excitation of fluorophores near and absorbed on the NR surface, further benefiting FE thereof. One paramount factor determining the waveguide properties of FPRs is the reflectance of the reflecting mirrors. Up to date, ZnO NR-based FE platform reported were produced on either Si wafers or glass slides<sup>6–8,17</sup>. Apparently, both substrates could restrict FE because Si has a much larger refractive index relative to ZnO as well as strong light absorption, and glass is highly transparent to visible and near-infrared light. To overcome the obstacle, employing a high-reflectance substrate would be more ideal.

In this work, ZnO NR arrays grown on pre-deposited Ag layers have been synthesized and employed as a new platform for high-sensitive fluorescence detection. Based on a direct comparison of NRs fabricated on patterned substrates with alternative Ag and bare Si striped zones, it has been revealed that FE factor of ZnO NRs on Ag can be significantly increased. The possible contributing factors involved in the enhancement, including the surface plasmons of Ag, reflectance of the substrates, the diameters of ZnO NRs and the associated guided fundamental mode and the high-ordered modes of the excitation light, are discussed accordingly.

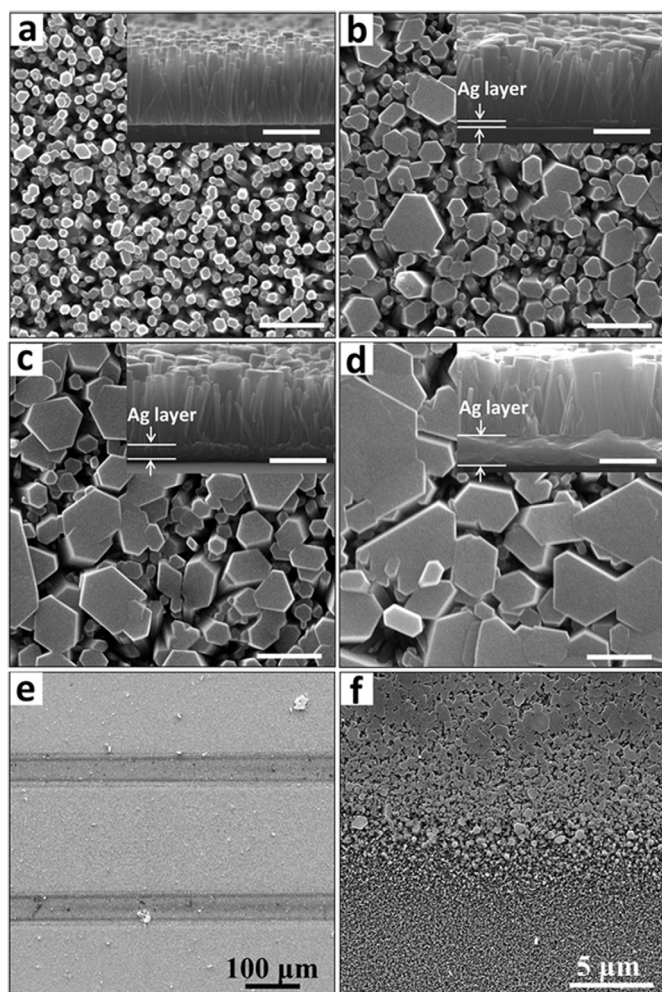


**Figure 1** | SEM images of ZnO NRs grown on Ag layers with different deposition durations of (a) 0 min (bare Si), (b) 5 min, (c) 10 min and (d) 30 min. (e) and (f) SEM images of ZnO NRs grown on Si substrate coated by patterned Ag layer deposited for 30 min. The scale bars in (a), (b), (c) and (d) are 500 nm.

## Results

Utilizing a sputtering method, Ag layers with three distinct thicknesses were introduced onto bare Si by varying the deposition duration. ZnO NRs were subsequently synthesized on the substrates using a hydrothermal method under the same preparation condition. Figure 1a–e present the top-view and cross-sectional (the inset) scanning electron microscopy (SEM) images of ZnO NR samples grown on bare Si, and Ag layers with the deposition durations of 5 min, 10 min and 30 min, producing a Ag layer with the thickness of 0 nm, ~60 nm, ~120 nm, and ~320 nm, respectively. The NRs are orientated perpendicular to the substrates into arrays in all cases; while extended deposition duration of Ag can lead to thicker NRs with a

constant length but a reduced number per unit area (See Figure S1 and Table 1). The crystalline nature of the samples was characterized by X-ray diffraction (XRD) in Figure S2. Fully consistent with SEM results, the dominated ZnO(002) peak also reveals the ordered alignment of the NRs for all samples, and the gradually magnified Ag(111) and Ag(200) peaks correspond to thickened Ag layers.

In order to directly compare FE of different ZnO samples, three patterned substrates with alternating Ag and bare Si zones were employed, which were achieved by using a copper grid for transmission electron microscopy as the mask and depositing Ag for 5 min, 10 min and 30 min, respectively. ZnO NR arrays were successively fabricated onto the substrates under the same seeding process and hydrothermal reaction conditions, exhibiting distinctive striped appearance thereof. SEM images in Figure 1e–f present examples of ZnO NRs grown on such substrates with 30-min deposition of Ag layer, showing that NRs on the Ag stripes (of ~200 μm wide) are remarkably thicker than those on the bare Si zones (of ~50 μm wide). The patterned ZnO samples were immersed into the same Rhodamine 6G (R6G) solution of  $10^{-6}$  M at 4°C for 12 h, then washed thoroughly by deionized water and dried in air. Figure 2a–c present the florescent images of R6G molecules on the patterned ZnO samples. It is found that the florescence intensity of R6G on the Ag-zone ZnO NRs is substantially higher than that on Si, among which 10-min deposited Ag layers produce the brightest fluorescence. Image analysis using Leica AF software reveal that the relative intensity of fluorescence signal from samples on the 5-min, 10-min, and 30-min deposited Ag layers is around 11, 47 and 25 times of that on the Si zone, as shown in Figure 2d. Bearing in mind that each ZnO sample has a different surface area, which primarily determines the amount of R6G molecules detected hence the fluorescence intensity, FE are therefore normalized by the total surface area of the NRs, resulting in an enhancement factor of 17, 86, and 69 for the three groups of Ag zones. FE of fluorescein isothiocyanate (FITC) molecules was examined on such patterned substrates as well (See Figure S3) and very similar results were obtained, confirming that the ZnO NRs/Ag can be an effective and universal FE platform for various molecular systems.

Since the morphology of ZnO NRs is modified accompanying with the variation of the Ag layers, i.e., the NRs on Ag layers are much thicker than those on bare Si, one could argue that the Ag layers beneath may not necessarily contribute to FE at all. To unambiguously clarify, a group of ZnO NR samples with similar average diameters, length and total surface area to the NRs grown on 30-min deposited Ag layers were synthesized on bare Si, as a comparison (See Figure S4). It is found that, with respect to the thinner NR samples, these thicker ones on Si indeed lead to an increased fluorescence, with a normalized enhancement factor of ~6, which is much smaller than NRs with similar morphology on Ag (6 vs. 69), relative to the same reference. This indicates that the Ag layers must have a significant contribution to the enhanced fluorescence of the NR/Ag samples.

As revealed in Figure S5, the as-deposited Ag layers contain many small Ag nanoparticles. It has been well demonstrated that the strong surface plasmon resonance of Ag nanoparticles could significantly

**Table 1** | Average length, density, relative fluorescence intensity and normalized enhancement factor of the ZnO NRs grown on the bare Si and pre-deposited Ag layers. Note that the statistical results of the NRs diameters are given in Figure S1

Substrate	Average Length (nm)	Estimated Surface Area of ZnO NRs per Unit Area ( $\mu\text{m}^2$ )	Relative Fluorescence Intensity	Normalized Enhance Factor
0-min Ag layer (bare Si)	~650	~22	1	1
5-min Ag layer	~650	~14	11	17
10-min Ag layer	~650	~12	47	86
30-min Ag layer	~650	~8	25	69

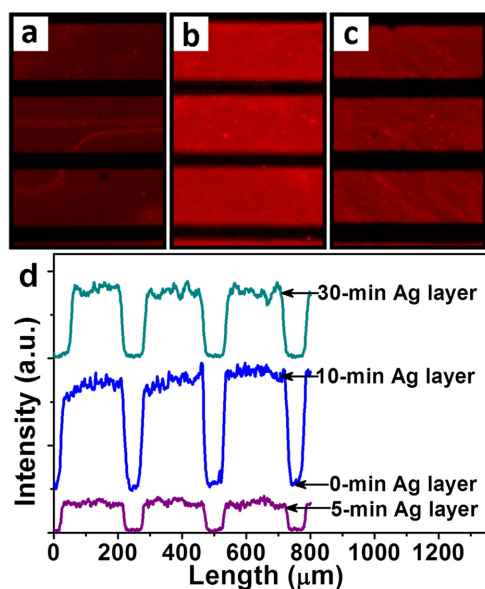


**Figure 2** | Fluorescence images of R6G molecules on ZnO NRs grown on patterned substrates with alternative stripes of bare Si and pre-coated Ag layer deposited for (a) 5 min, (b) 10 min and (c) 30 min. (d) Fluorescence intensity across the NR patterns, where for all curves the top flat section corresponds to the Ag zone and the low-lying part to Si area.

contribute to the fluorescence enhancement of the fluorophores<sup>18,19</sup>. However, there is a precondition for such an enhancement, i.e. the coupling distance between the metal substance and the fluorophores has to be shorter than  $20 \text{ nm}^1$ . In this work, this condition is obviously not satisfied, because the Ag layers are fully covered by a ZnO seed layer and a close-packed ZnO nanorod (NR) array subsequently. Therefore, the impact of surface plasmons induced by Ag layers on fluorophores should be very limited, hence can not be the primary cause of the greatly enhanced FE.

It is worthy to mention that, unlike Si, which is instinctively prone to trap light given its high refraction index, Ag has a strong capability of reflecting and scattering light<sup>20</sup> and has been widely applied as back reflector in solar cells<sup>21</sup>. Figure 3 presents diffuse reflectance of ZnO NRs grown on different substrates, where the reflectance of ZnO NRs on all Ag layers is larger than 80% for light with wavelength  $>500 \text{ nm}$ , which is much higher than that on Si ( $\sim 53\%$ ). Since ZnO is highly optical-transparent for light with wavelength  $>400 \text{ nm}$ , the relative low reflectance on bare Si is mainly attributed to the light absorption of Si substrate, while the addition of Ag layer is responsible for the much enhanced reflectance of the ZnO NRs grown on different Ag layers in the wavelength range of  $500\text{--}800 \text{ nm}$ . This can

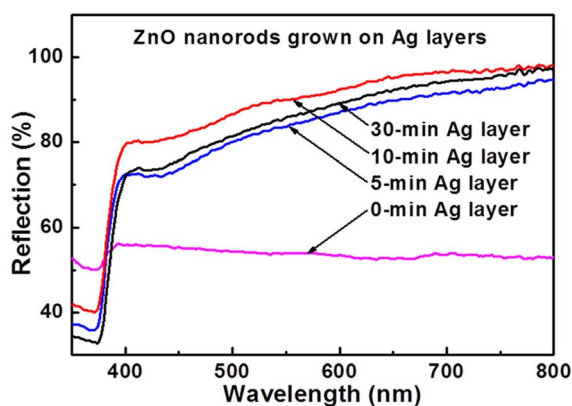


**Figure 3** | Diffuse reflectance of ZnO NRs grown on different substrates.

benefit the waveguide of ZnO NRs on both the excitation light ( $\sim 527 \text{ nm}$ ) and the fluorescence of R6G molecules ( $\sim 555 \text{ nm}$ ). The guided fundamental mode and the high-order modes of the excitation light are capable to strengthen local or evanescent field in the vicinity of NRs, remarkably enhance the excitation of the fluorophores. Furthermore, the emission light from the fluorophores can be captured and guided to propagate along the  $c$ -axis of the NRs, and finally emitted from the top of the NRs. In this way, the fluorescence signal is more likely and facile to be captured by the detector located above the samples.

## Discussion

The similar reflectance but very different normalized FE factors of ZnO NRs on different Ag layers can be assigned to the NR diameter disparity. Besides the surface area to volume ratio, the NR diameter also has a critical influence on the waveguide properties of NR-like structures. The evanescent field is raised from high-mode waveguiding, which require the NR diameter meets the condition of  $2\pi r/\lambda_0(n_1^2 - n_{\text{air}}^2)^{1/2} > 2.405$ , where  $r$  is the NR radius,  $\lambda_0$  is the vacuum wavelength, and  $n_1$  and  $n_{\text{air}}$  are the refractive indices of ZnO and air, respectively<sup>22</sup>.

According to the calculations, with a given excitation light of  $\sim 527 \text{ nm}$ , the evanescent field of the multimode waveguide only occurs for NRs thicker than  $\sim 220 \text{ nm}$ , otherwise only the contribution from the fundamental mode can be taken into account. A statistic analysis based on SEM results (Figure S1) reveals that  $\sim 5\%$ ,  $\sim 25\%$  and  $\sim 65\%$  of NRs grown on 5-min, 10-min, and 30-min deposited Ag layers are thicker than  $\sim 220 \text{ nm}$ , respectively. Compared with the sample on 5-min deposited Ag layer, the much larger FE factor on 10-min deposited Ag layers indicates that the guided high-order modes have larger contributions than that of the fundamental mode. In this rationale, one would expect that the samples on the 30-min deposited Ag layers would induce an even higher enhancement, which is in conflict with the experimental results. Fortunately, it was reported previously that the intensity and the penetration depth of the evanescent field around the ZnO NRs decrease with the increase of NR diameter<sup>15</sup>. This means that, although NR diameters larger than  $220 \text{ nm}$  may provide benefits, further expansion can severely weaken the enhancement. Therefore, an optimum condition for the highest FE factor exists. These results may provide a deep insight on the mechanism of NRs-based FE platform, and pave the way for better structure design and property optimization.

## Methods

**Deposition of Ag layers.** Ag layers were introduced on Si (100) substrates by a radio frequency (RF) magnetron sputtering technique. In short, Ag target (99.99%) was sputtered at room temperature with RF power of  $100 \text{ W}$ , environment gas pressure of  $1 \text{ Pa}$  (argon gas with a flow rate of  $40 \text{ sccm}$ ), distance between the target and the substrate of  $5 \text{ cm}$ , and the durations are: 5, 10 and 30 min respectively. In order to obtain patterned substrates, striped copper transmission electron microscopy grids (100 meshes) were employed as masks and mounted on the Si substrate before the Ag deposition.

**Synthesis of ZnO nanorods.** A thin ZnO seed layer was deposited on the Ag-coated Si substrate before the hydrothermal growth of ZnO nanorods. The ZnO seeds were formed by sputtering ZnO ceramic target (99.99%) at the temperature of  $400^\circ\text{C}$  with RF power of  $150 \text{ W}$ , environment gas pressure of  $1 \text{ Pa}$  (argon and oxygen gas with flow rate of 40 and  $10 \text{ sccm}$ , respectively) and fixed target-substrates distance of  $5 \text{ cm}$  for 2 min. For hydrothermal growth of ZnO nanorods,  $50 \text{ mL}$  Zinc nitrate hexahydrate solution ( $\text{Zn}(\text{NO}_3)_2 \cdot 6\text{H}_2\text{O}$ , 99%, Aladdin, China,  $0.1 \text{ M}$ ) and  $50 \text{ mL}$  hexamethylenetetramine solution (HMT,  $\text{C}_6\text{H}_{12}\text{N}_4$ , 99%, Aladdin, China,  $0.1 \text{ M}$ ) were pre-heated at  $92^\circ\text{C}$  and then were mixed together in a glass bottle of maximum volume  $130 \text{ mL}$ , the substrates of interest were immediately immersed in this reactive solution, and the bottle was then sealed and held at a constant temperature ( $92^\circ\text{C}$ ) for 3 h. The as-formed ZnO nanorod samples were cleaned by rinsing with deionizer water and ethanol, and then dried in air.

**Evaluation of fluorescence enhancement.** Fluorescent probes R6G (Aladdin, China) and FITC (Aladdin, China) were dissolved in deionized water. The as-prepared ZnO nanorod samples were immersed in the dye solutions ( $20 \mu\text{g mL}^{-1}$  FITC and  $10^{-6} \text{ M}$  R6G) at  $4^\circ\text{C}$  for 12 h. After thoroughly washed by deionizer water, these samples were



dried in air before the fluorescence measurements. The fluorescent images of different samples modified with the same fluorophore were taken under the same condition by a fluorescence microscope (Leica DM4000 B). FITC molecules were excited at  $480 \pm 20$  nm and exposed for 1 s, and R6G molecules were excited at  $527 \pm 15$  nm with an exposure time of 200 ms. All obtained fluorescence results were analyzed by the Leica AF software.

**Characterizations.** Morphologies and crystallization nature of the products were characterized by SEM (FEI Quanta 200F, 30 kV) and XRD (PANalytical, X'Pert Pro, with Cu K $\alpha$  radiation). The diffusion reflection spectra were measured in a U4100 UV-vis-NIR spectrometer (Hitachi) equipped with integrating sphere in the wavelength range of 350–800 nm.

- Hao, Q., Qiu, T. & Chu, P. K. Surface-enhanced cellular fluorescence imaging. *Prog. Surf. Sci.* **87**, 23–45 (2012).
- Hahn, J. Zinc oxide nanomaterials for biomedical fluorescence detection. *J. Nanosci. Nanotechnol.* **14**, 475–486 (2014).
- Wells, S. M., Merkulov, I. A., Kravchenko, I. I., Lavrik, N. V. & Sepaniak, M. J. Silicon nanopillars for field-enhanced surface spectroscopy. *ACS Nano* **6**, 2948–2959 (2012).
- Xie, C., Hanson, L., Cui, Y. & Cui, B. Vertical nanopillars for highly localized fluorescence imaging. *PNAS* **108**, 3894–3899 (2011).
- Kandziolka, M. *et al.* Silicon nanopillars as a platform for enhanced fluorescence analysis. *Anal. Chem.* **85**, 9031–9038 (2013).
- Kumar, N., Dorfman, A. & Hahn, J. Ultrasensitive DNA sequence detection using nanoscale ZnO sensor arrays. *Nanotechnology* **17**, 2875–2881 (2006).
- Dorfman, A., Kumar, N. & Hahn, J. Highly sensitive biomolecular fluorescence detection using nanoscale ZnO platforms. *Langmuir* **22**, 4890–4895 (2006).
- Hu, W., Liu, Y., Yang, H., Zhou, X. & Li, C. M. ZnO nanorods-enhanced fluorescence for sensitive microarray detection of cancers in serum without additional reporter-amplification. *Biosens. Bioelectron.* **26**, 3683–3687 (2011).
- Fu, Y., Zhang, J. & Lakowicz, J. R. Photophysical behaviors of single fluorophores localized on zinc oxide nanostructures. *Int. J. Mol. Sci.* **13**, 12100–12112 (2012).
- Kim, J., Kwon, S., Park, J.-K. & Park, I. Quantum dot-based immunoassay enhanced by high-density vertical ZnO nanowire array. *Biosens. Bioelectron.* **55**, 209–215 (2014).
- Adalsteinsson, V. *et al.* Ultrasensitive detection of cytokines enabled by nanoscale ZnO arrays. *Anal. Chem.* **80**, 6594–6601 (2008).
- Sirbully, D. J., Tao, A., Law, M., Fan, R. & Yang, P. Multifunctional nanowire evanescent wave optical sensors. *Adv. Mater.* **19**, 61–66 (2007).
- Yan, R., Gargas, D. & Yang, P. Nanowire photonics. *Nat. Photonics* **3**, 569–576 (2009).
- Seo, K. *et al.* Multicolored vertical silicon nanowires. *Nano Lett.* **11**, 1851–1856 (2011).
- Börner, S., Rüter, C. E., Voss, T., Kip, D. & Schade, W. Modeling of ZnO nanorods for evanescent field optical sensors. *Phys. Stat. Sol. (a)* **204**, 3487–3495 (2007).
- Voss, T. *et al.* High-order waveguide modes in ZnO nanowires. *Nano Lett.* **7**, 3675–3680 (2007).
- Hu, W., Liu, Y., Zhu, Z., Yang, H. & Li, C. M. Randomly oriented ZnO nanorods as advanced substrate for high-performance protein microarrays. *ACS Appl. Mat. Interfaces* **2**, 1569–1572 (2010).
- Li, H., Qiang, W., Wang, C., Vuki, M. & Xu, D. Ultrasensitive and fast fluorescent bioassay based on fluorescence enhancement of silver nanoparticles. *Analyst* **138**, 7376–7383 (2013).
- Fang, X. *et al.* Nanoscale control of Ag nanostructures for plasmonic fluorescence enhancement of near-infrared dyes. *Nano Research* **6**, 496–510 (2013).
- Jung, Y. S. Study on texture evolution and properties of silver thin films prepared by sputtering deposition. *Appl. Surf. Sci.* **221**, 281–287 (2004).
- Söderström, K. *et al.* Highly reflective nanotextured sputtered silver back reflector for flexible high-efficiency n-i-p thin-film silicon solar cells. *Sol. Energy Mater. Sol. Cells* **95**, 3585–3591 (2011).
- Tong, L., Lou, J. & Mazur, E. Single-mode guiding properties of subwavelength-diameter silica and silicon wire waveguides. *Opt. Exp.* **12**, 1025–1035 (2004).

## Acknowledgments

This work was financially supported by the National Natural Science Foundation of China (Grant No.11104046), National Basic Research Program of China (973 Program) (Grant No. 2013CB632900), the Fundamental Research Funds for the Central University (Grant Nos. HIT.BRETHI.201216, HIT.BRETHI.201225, and HIT.BRETHI.201313). M.Y. thanks financial support by the Young Thousand Talent Plan.

## Author contributions

Y.Y. carried out the experiments and performed the data analysis. Y.S. and M.Y. designed the experiments, helped with the data discussion and interpretation, and were the main authors of the article. X.L. and T.J. contributed synthesis and characterization of the ZnO samples. D.L. and S.L. assisted with the diffuse reflectance measurement. B.Y. assisted with the seed layer growth. W.C. contributed to interpretation of data and revision of the article.

## Additional information

**Supplementary information** accompanies this paper at <http://www.nature.com/scientificreports>

**Competing financial interests:** The authors declare no competing financial interests.

**How to cite this article:** Yin, Y. *et al.* ZnO Nanorod Array Grown on Ag Layer: A Highly Efficient Fluorescence Enhancement Platform. *Sci. Rep.* **5**, 8152; DOI:10.1038/srep08152 (2015).



This work is licensed under a Creative Commons Attribution-NonCommercial-ShareAlike 4.0 International License. The images or other third party material in this article are included in the article's Creative Commons license, unless indicated otherwise in the credit line; if the material is not included under the Creative Commons license, users will need to obtain permission from the license holder in order to reproduce the material. To view a copy of this license, visit <http://creativecommons.org/licenses/by-nc-sa/4.0/>